ACS OMEGA

Open Access

http://pubs.acs.org/journal/acsodf

Article

Thorium Complexation with Aliphatic and Aromatic Hydroxycarboxylates: A Combined Experimental and Theoretical Study

Pranaw Kumar, Rama Mohana Rao Dumpala, Vijay M. Telmore, Biswajit Sadhu, Mahesh Sundararajan,* Ashok K. Yadav, D. Bhattacharyya, and Jaison P. George*

Cite This: *ACS Omega* 2024, 9, 27289−27299

Read Online

ACCESS | Metrics & More | Article Recommendations | Supporting Information

ABSTRACT: Hydroxycarboxylic acids, viz., α-hydroxyisobutyric acid (HIBA) and mandelic acid (MA), have been widely employed as eluents for inner transition metal separation studies. Both extractants have identical functional groups (OH and COOH) with different side-chains. Despite their similarities in binding motifs, they show different retention behaviors for thorium and uranium in liquid chromatography. To understand the mechanism behind the trend, a detailed study on the aqueous phase interaction of thorium with both extractants is carried out by speciation, spectroscopy, and density functional theory-based calculations. Potentiometric titration experiments are carried out to reveal the stability and species formed. Electrospray ionization mass spectrometry is performed to identify the formation of different species by Th with both HIBA and MA. It is seen that for Th-HIBA and Th-MA, the dominating species are ML_3 and ML_4, respectively. A similar pattern observed in potentiometric speciation analysis supports the tendency of Th to form higher stoichiometric species with MA than with HIBA. The difference in the dominating species thus helps in explaining the reversal in the retention behavior of uranium and thorium in the reverse-phase liquid chromatographic separation. The results obtained are corroborated with extended X-ray absorption fine structure spectroscopic measurements and density functional theory (DFT) calculations.

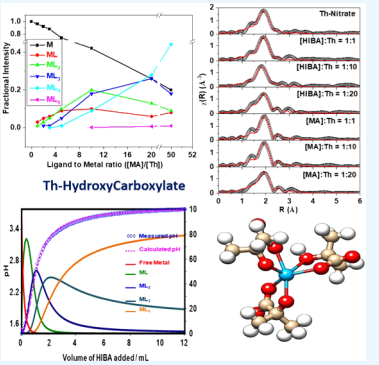

1. INTRODUCTION

Safe handling of spent nuclear fuel and efficient radioactive waste management are the key concerns for progressive nuclear energy and its public acceptance. Actinides, due to their long radioactive lifetime, need prior isolation to minimize the radiochemical hazard to the environment and to ease the waste management protocols.[1] Thus, the separation of actinides and lanthanides is the central step for successful nuclear fuel reprocessing. Further, the separation of trivalent actinides and lanthanides is difficult due to the similarities in the physiochemical properties. Researchers have developed the ligands utilizing the principle of hard−soft acid−base for the separation of An(III) and Ln(III). Diamide ligand-based extractants, where the presence of nitrogen provides softness, are used for the separation of An(III) and Ln(III).[2−6] Hydroxycarboxylic acids, namely, α-hydroxyisobutyric acid (HIBA)[7−12] and mandelic acid (MA) (Scheme 1), have been well-known eluting reagents for the liquid chromatographic separation of actinides and lanthanides.[13−15] Reports showed that the elution pattern changes in order by the application of HIBA instead of MA and vice versa. Both HIBA and MA bind the metal ions through the same functional moieties but differ in their side-chains. HIBA and MA possess an aliphatic dimethyl group and aromatic phenyl ring as side-chains, respectively. Thorium elutes before uranium by HIBA, whereas the elution pattern is reversed on using MA in reverse-phase chromatographic separation.[16]

Scheme 1. Schematic Representation of Hydroxycarboxylic Acid: (A) HIBA and (B) MA

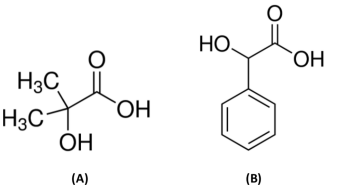

Carboxylate and hydroxyl groups are primary coordinating moieties for metal ions in most of the natural organic matter such as humic substances.[17−20] Further, hydroxyl and carboxylate groups are known for their vast applications in the fields of polymers, food, fabrics, and pharmaceuticals.[21−25]

Received: February 19, 2024
Revised: May 31, 2024
Accepted: June 5, 2024
Published: June 13, 2024

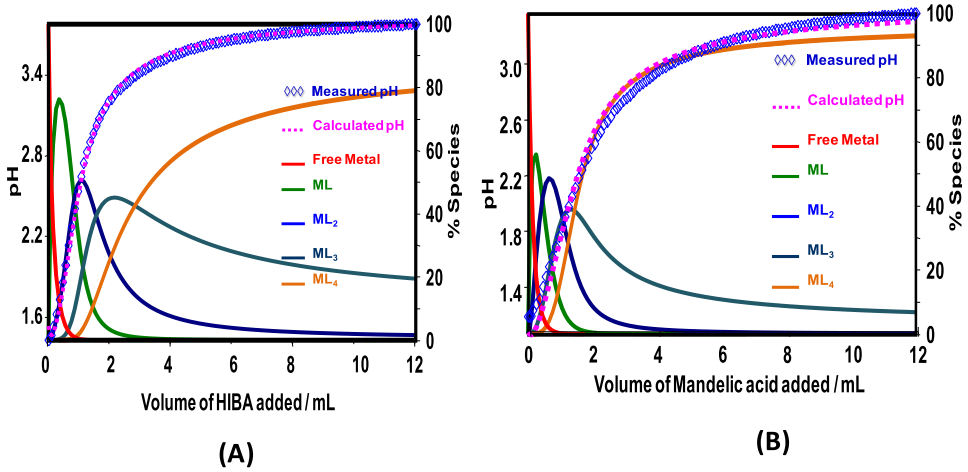

Figure 1. Speciation plots along with the fitted data for pH measurements: (A) Th-HIBA complexation and (B) Th-MA complexation; at T = 298 K, P = 0.1 MPa. [Th(IV)] = 0.003 M; [HIBA/MA] = 0.3 M.

HIBA is an essential raw source for syntheses of key amino acids such as isoleucine, polymeric hydroxyl carboxylic acid, and antibiotic and antitumor medicines.[26−28] The MA degradation path is proven to be representative of most of the aromatic substances in nature.[29] MA is also known for its antimicrobial characteristics and, due to its nontoxic behavior, is widely used in the pharmacokinetic industry specifically to treat urinary tract infections.[30] Thus, both HIBA and MA serve as key models to study the interaction of radiotoxic metal ions such as thorium, as in the present study.

Aqueous speciation and structural elucidation in terms of coordination modes and stoichiometry of Th(IV) complexes have proven to be beneficial in understanding the mechanism behind the differential complexing pattern. Magon et al. studied the speciation of thorium by three isomeric HIBA by potentiometry and reported the formation and stability of four consecutive species, namely, ML_1 to ML_4, for Th-HIBA/MA complexes,[31] while Portanova et al. compiled the stability constants for the Th-HIBA system under different experimental conditions.[32] There are several reports on the effective use of HIBA and MA as separation agents for lanthanide or lanthanide−actinide mixtures in solutions.[8−16,33] Datta et al. attempted to correlate the stability and speciation of Ln(III)/An(III) with HIBA/MA, whereas the corresponding tetravalent actinides, such as Th(IV), were not investigated. The necessity for comprehensive speciation by a combination of experimental and theoretical viewpoints motivated us to carry out a detailed speciation investigation for the Th-HIBA/MA system. In the present study, potentiometric titrations are performed to determine the species formed during the course of the reaction as well as the corresponding thermodynamic stabilities. The physical verification and validations of various species are confirmed by electrospray ionization mass spectrometry (ESI-MS). The local structure was probed by X-ray absorption measurement to obtain knowledge on the coordination atoms as well as the coordination number around Th(IV) ions. Finally, density functional theory (DFT)-based calculations were carried out to understand the complexation process at the molecular level. Our computational estimation matches well with our experimental estimates of ESI-MS, potentiometric, and extended X-ray absorption fine structure (EXAFS) data. To the best of our knowledge, this is the first attempt in the literature to determine the speciation and structural elucidation of Th-HIBA/MA complexes to interpret the elution patterns.

2. EXPERIMENTAL DETAILS

2.1. Reagents. Thorium (inductively coupled plasma-MS (ICP-MS) standard from Inorganic Ventures, Bengaluru, India) and thorium nitrate salt were used to prepare the thorium stock solution. α-Hydroxyisobutyric acid (99% purity, Alfa Aesar), mandelic acid (99% purity, Sigma-Aldrich), methanol (UHPLC grade, Sigma-Aldrich), and nitric acid (70% ACS reagent, Sigma-Aldrich) were used as such for reagent and sample preparations.

2.2. Instrumentation. ESI-MS (model micrOTOFQ-II, BrukerDaltonics GmbH), assisted by Bruker Compass Data Analysis software and Compass Isotope Pattern software, was performed for the physical identification of the species. An autotitrator (Metrohm; 905 Titrando model) was used to carry out all of the potentiometric titrations. Extended X-ray absorption fine structure (EXAFS) at Th L3 edges was carried out at the energy-scanning EXAFS beamline (BL-9) of the Indus-2 Synchrotron Source (2.5 GeV, 100 mA), Raja Ramanna Centre for Advanced Technology (RRCAT), Indore, India.[34,35]

2.3. Computational Protocol. To gain molecular-level geometrical insights on the speciation of Th(IV) ion with HIBA and MA, density functional theory (DFT) calculations were carried out. In this way, our computed geometric species can be gauged with the experimentally estimated EXAFS structural parameters and ESI-PES stoichiometric species.

All structures are optimized with the BP86 functional[36−38] in conjunction with the def2-TZVP basis set for all atoms except Th. For Th(IV) ions, a def-TZVP basis set is used. The importance of weak interactions is recognized, and thus, dispersion corrections are incorporated through Grimme's D3BJ empirical corrections.[39,40] Vibrational frequency calculations are carried out to verify the optimized structure minima and extract the thermodynamic parameters at room temperature (T = 298.15 K) for the computation of Gibbs free energies. As the Hartree−Fock exchange terms significantly contribute to the energetics, single-point calculations of all species are computed at the B3LYP/def2-TZVP (Th = def-TZVP) level. As ESI-MS data are in the gas phase and potentiometric measurements are performed in the aqueous

https://doi.org/10.1021/acsomega.4c01581
ACS Omega 2024, 9, 27289−27299

phase, a continuum solvation model (COSMO) with ε = 80 (dielectric constant of water) is used to correct the gas phase free energies.[41−43] We successfully used this strategy for several speciation studies involving heavy metal ions, including those of actinide ions.[44−46] All calculations are performed with TURBOMOLE 7.2.[47,48]

3. RESULTS AND DISCUSSION

3.1. Aqueous Speciation and Complexation Stability.

Upon complexations, extractants with dissociable protons are prone to protonation and deprotonation, and thus, a change in the hydrogen ion concentration (pH) is a good indicator of complexation progress.[49−63] In the present study, the sequential progress of complexation is probed by adding a concentrated ligand solution into a fixed concentration of a metal solution and monitoring the pH after each addition of the ligand. Potentiometric data were analyzed by Hyperquad program[64,65] to deduce the species present along with stability for complex formation during the course of the reaction. Speciation plots (Figure 1) showed that Th(IV) forms ML_i (i = 1−4) complexes with both extractants.

The pK_a of HIBA is 3.8, whereas for mandelic acid, it is 3.4.[66,67] At pH 5.0, which is slightly higher than the pK_a values of both acids, both will exist predominantly in their deprotonated forms. However, as mandelic acid has a lower pK_a than HIBA, it will have a higher percentage of its molecules in the deprotonated form at pH 5.0. This means that mandelic acid will have a greater ability to form stoichiometric complexes compared to HIBA at pH 5.0 due to the higher percentage of its molecules being in the ionized form (Figure S1). This difference in the ionization behavior might be influencing their ability to form complexes. Although the kind of species formed is the same in both systems, three major differences could be observed from speciation plots, as shown in Figure 1. First, ML_1 formation is relatively higher for Th-HIBA than for the Th-MA complex (green color). Second, ML_4 formation (orange color) starts relatively earlier for the Th-MA complex than for the Th-HIBA complex. Finally, ML_3 formation (violet color) is relatively higher for Th-HIBA than for Th-MA, while the opposite is true for ML_4 formation at the end of titration.

HIBA contains an aliphatic moiety that allows flexibility in coordinating with the metal ion, whereas MA contains a more preordered structure due to its rigid phenyl ring. Because of this rigidity in the structure of MA, it requires certain specific configurations before binding with the metal. This caused the Th-HIBA complex to be more stable than the Th-MA complex (Table 1). A similar effect was previously observed for Th-acetate and Th-benzoate systems. The thermodynamic stabilities ($\log\beta$) of Th(IV) ion with HIBA and MA are shown in Table 1. Except for ML_4, $\log\beta$ values are higher for HIBA compared to MA, and the formation of ML_4 starts early in speciation plots for Th-MA than for the Th-HIBA system. Further, the difference in $\log\beta$ for ML_4 from ML_3 formation is higher for the Th-MA system ($\Delta\log\beta$ = 2.18) than for the Th-HIBA system ($\Delta\log\beta$ = 1.86), resulting in the favorable formation of ML_4 from ML_3 for Th(IV) ion interaction with MA compared to HIBA. Hence, the fractional availability of ML_4 with respect to ML_3 would be higher for Th-MA complexes than for Th-HIBA. ML_4 is a neutral complex, while ML_3 is a monopositive ion. For the Th-MA system, the neutral fraction (ML_4) would be high, hence resulting in a strong low retention and later elution compared to HIBA under reverse-phase chromatographic conditions.

Table 1. Thermodynamic Stability ($\log\beta$) of Th(IV) Ions with HIBA and MA at T = 298 K and P = 0.1 MPa[a]

	$\log\beta$	
reaction	HIBA	MA
$H + L^- \leftrightarrow LH$	3.77 ± 0.01	3.26 ± 0.01
$M + L^- \leftrightarrow ML^{3+}$	4.67 ± 0.01	4.07 ± 0.01
$M + 2L^- \leftrightarrow ML_2^{2+}$	7.73 ± 0.01	7.27 ± 0.01
$M + 3L^- \leftrightarrow ML_3^{+}$	10.11 ± 0.01	9.80 ± 0.01
$M + 4L^- \leftrightarrow ML_4$	11.97 ± 0.01	12.08 ± 0.01

[a] $[Th^{4+}]$ = 0.003 M; [HIBA/MA] = 0.3 M.

3.2. Species Identification by ESI-MS. *3.2.1. Th-HIBA Speciation.* ESI-MS in both positive and negative ion modes was employed to identify the species formed by thorium with HIBA and MA. The formation of possible species of ML_3 and ML_4 by HIBA in positive ion mode is shown in Table 2,

Table 2. Positively Charged Species of Th (2×10^{-6} M) with HIBA (4×10^{-5} M) and HNO_3 (2×10^{-5} M) in MeOH Medium

stoichiometry	species	m/z	relative abundance (%)
ML_1	$[ThO(C_4H_7O_3)]^+$	351.07	14.91
	$[Th(C_4H_7O_3)(OH)(NO_3)]^+$	414.07	25.72
	$[Th(OH)(C_4H_7O_3)_2]^+$	455.11	11.86
	$[Th(C_4H_7O_3)(NO_3)_2]^+$	459.06	15.54
	$[Th(C_4H_7O_3)(NO_3)_2(H_2O)]^+$	477.07	18.26
	$[Th(C_4H_7O_3)(NO_3)_2(H_2O)_2]^+$	495.08	13.76
	$[Th(C_4H_7O_3)(H_2O)_3(NO_3)_2]^+$	513.17	10.0
ML_2	$[Th(OH)_2(C_3H_6O)(C_4H_7O_3)]^+$	427.12	18.0
	$[Th(C_4H_7O_3)(C_4H_6O_3)]^+$	437.10	2.54
	$[Th(OH)(C_4H_7O_3)_2(H_2O)]^+$	473.13	12.63
	$[Th(C_4H_7O_3)_2(NO_3)]^+$	500.1	34.05
	$[Th(C_4H_7O_3)_2(H_2O)(NO_3)]^+$	518.11	39.63
ML_3	$[Th(C_4H_7O_3)_3]^+$	541.16	100
	$[Th(C_4H_7O_3)_3(H_2O)]^+$	559.16	11.04
	$[Th(C_4H_7O_3)_2(C_4H_8O_3)(NO_3)]^+$	604.16	82.7
ML_4	$[Th(C_4H_7O_3)_3(C_4H_8O_3)]^+$	645.20	52.22

whereas in Table S1, possible species in negative modes are shown in the electronic Supporting Information. HIBA has two dissociable protons as carboxylic acid and hydroxyl functional groups, and thus, ESI-MS could identify a number of species by permutations of different protonated/deprotonated groups with varying stoichiometries (ML_1, ML_2, ML_3, ML_4). HIBA ($C_4H_8O_3$) in the completely dissociated form as $(C_4H_6O_3)^{2-}$ or in the partially dissociated form as $(C_4H_7O_3)^{1-}$ would interact with Th(IV) ion to form complexes with different stoichiometric ratios, as presented in Scheme S1.

In the negative ion mode, the maximum number of HIBA present around Th(IV) is 5, and the formation of different stoichiometries of metal−ligand complexes was proposed as a stepwise replacement of nitrate by the HIBA moiety (Scheme

https://doi.org/10.1021/acsomega.4c01581
ACS Omega 2024, 9, 27289−27299

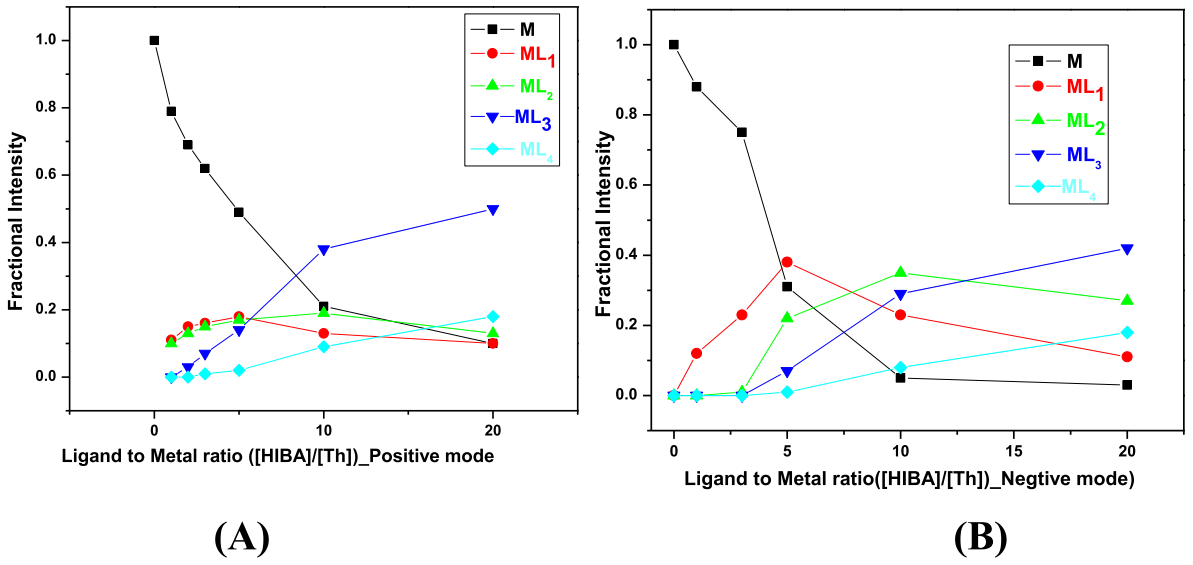

Figure 2. Thorium-HIBA speciation with varying ligand/metal ratios ([HIBA]/[Th]) in (A) positive and (B) negative ion modes.

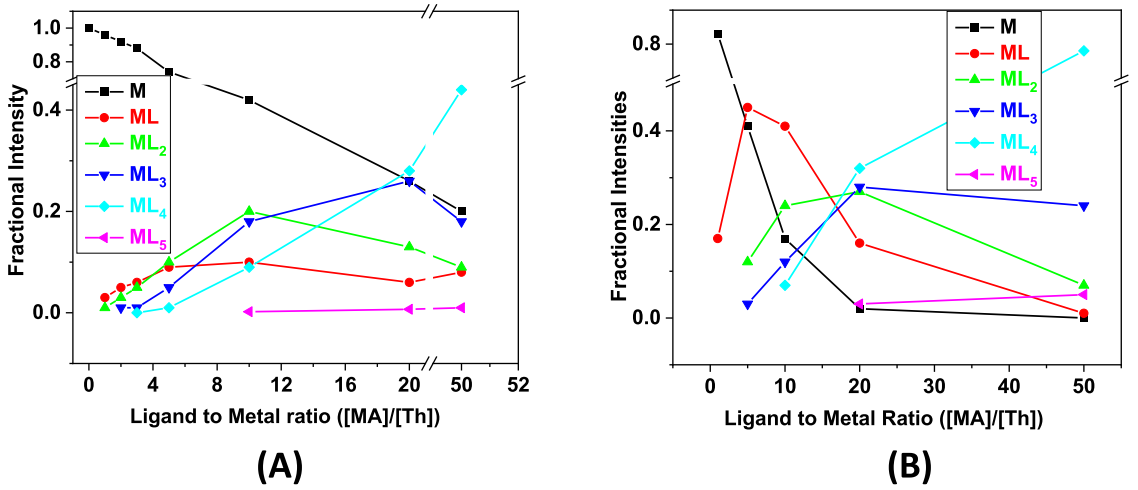

Figure 3. Thorium-MA speciation with varying ligand/metal ratios ([MA]/[Th]) in the (A) positive and (B) negative ion modes.

S2). Here, similar to the previously reported studies of uranyl-HIBA and uranyl-MA, the negative ion species of Th-HIBA were deprived of methanol.

3.2.2. Th-MA Speciation. Similar to the Th-HIBA system, different species formed by Th(IV) ion with MA in ML_3 to ML_5 types in both positive and negative ion mode are shown in Tables S2 and S3, respectively. It was observed that at an L/M ratio of 20, in the case of MA, the ML_4 species ($[Th(C_8H_7O_3)_3(C_8H_8O_3)]^+$) was the most dominating, which is in contrast to the trend observed in the Th-HIBA system under similar conditions. Similarly, the ML_5 type of species, viz., $[Th(C_8H_7O_3)_3(C_8H_8O_3)_2]^+$, was also found with a very low relative intensity of ~5%, whereas no such ML_5 type species was observed in the case of the Th-HIBA system. The formation of these species was considered as a stepwise replacement of the nitrate moiety by MA, as shown in Schemes S3 and S4 in the Supporting Information.

In order to obviate artifact formation during the ESI process, the mass spectrum was also recorded in the negative ion mode. In the negative ion mode, the ML_5 type of species was observed for MA. All of the species were singly charged monomeric species with the double deprotonation of MA and nitrate as the chelating ligand. It is important to mention here that nitrate-containing species were found to be dominating in negative ion mode. However, $[Th(C_8H_7O_3)_3(C_8H_6O_3)]^-$ was the base peak in the Th-MA acid system, and this observation is in contrast to the trend observed in the negative ion mode with the Th-HIBA system, which showed $[Th(C_4H_6O_3)(C_4H_7O_3)_2(NO_3)]^-$ as the base peak under similar conditions.

3.3. Equilibrium Studies with Changes in the Ligand/Metal Ratio (L/M). *3.3.1. Th-HIBA System.* In order to study the equilibrium of the complexation of Th with HIBA, the ligand/metal ratio (L/M) was varied for the fixed metal concentration in both the positive and negative ion modes. Figure 2(A,B) shows the change in fractional intensities of uncomplexed Th ions and complexed Th-HIBA species as a function of the L/M ratio in both positive and negative ion modes. The uncomplexed metal ion intensities are the summation of all of the solvated species of thorium, viz., $[ThO(OH)]^+$,$[Th(OH)_3]^+$, $[Th(OH)_2(CH_3O)]^+$, $[Th(OH)_2(NO_3)]^+$, etc., in the positive ion mode. Similarly, the fractional intensities of complexed species, e.g., ML_1 in the positive ion mode, are a summation of fractional intensities of all possible species, viz., $[ThO(C_4H_7O_3)]^+$, $[Th(C_4H_7O_3)$-

https://doi.org/10.1021/acsomega.4c01581
ACS Omega 2024, 9, 27289−27299

$(OH)(NO_3)]^+$, $[Th(C_4H_7O_3)(NO_3)_2]^+$, etc., associated with ML_1. At a lower L/M ratio, the uncomplexed Th-solvated species are more dominating over the Th-HIBA species. Among the Th-HIBA complexed species at a lower stoichiometry, ML_1 and ML_2 were dominating over the bulkier species. At L/M $\geq$ 10, the ML_3 species was the most dominating over the other uncomplexed and complexed species. Similarly, in negative ion mode, at lower L/M ratios, the uncomplexed species were dominating, which reduced with an increase in the L/M ratio. The dominance of ML_3 species over ML_4 in the case of Th-HIBA complexation studies is clearly observed.

3.3.2. Th-MA Species. In order to verify the representation of the solution chemistry in the gas phase, the ligand/metal (L/M) ratios were varied from 1 to 50. The distribution of the species calculated in terms of fractional intensities was plotted as shown in Figure 3(A,B). It was observed that at lower L/M ratios (L/M = 2), the fractional intensities of unbound metal and ML_1-type species were dominating over the other species, whereas with an increase in the L/M ratio, the intensities of the complexes with a higher number of ligand species were found to increase. Further increase in the L/M ratio (L/M $\geq$ 20) led to the most dominating species as ML_4. Interestingly, after an L/M ratio of 10, ML_5 species are seen in ESI-MS, which is in contrast to the pattern observed with the Th-HIBA complex, which did not show any ML_5-type species. As a higher number of ligands are required, the higher stoichiometric complexes depend upon the L/M ratios and the stability constants of different species that are also responsible for the change in fractional intensities. Hence, the change in intensities of the complex species in the ESI-MS spectrum with the change in the L/M ratio indicates the progression of complexation and representation of solution chemistry in the gas phase. Also, the dominance of $[Th(MA)_4]$ species corroborates the more hydrophobic nature of the species, which in turn reflects the strong retention in liquid chromatographic conditions. The liquid chromatographic separation of Th and uranium onto the RP column using MA showed a higher retention of Th compared to U, whereas the retention trend is reversed when HIBA is used as the eluent.

For the Th-HIBA system, in both positive and negative ion modes, ML_3 species were found to be more abundant among all other species, while for the Th-MA system, ML_4 is the most abundant species among all other species. Further, negatively charged ML_5 species were observed for the Th-MA system in both modes, whereas species beyond ML_4 are absent in the case of the Th-HIBA system. Thus, the fractional availability of positively charged ML_3 species is predominant for the interaction of thorium with HIBA, whereas MA interaction with thorium favors either neutral ML_4 species or negatively charged ML_5 species. Hence, MA species would have stronger retentions and delayed elution for thorium compared to HIBA species.

3.4. X-ray Absorption Spectroscopy (XAS) Studies. The local structure around Th was obtained from the quantitative analysis of EXAFS spectra at Th L3 edges to deduce the coordination number and coordinating atoms in Th-HIBA/MA species. In order to take into consideration the oscillations in the absorption spectra, the atomic background function $\mu(E)$ was converted to absorption function $\chi(E)$, defined as follows[68]

$$\chi(E) = \frac{\mu(E) - \mu_0(E_0)}{\Delta\mu_0(E_0)}$$

where E_0 is the absorption edge energy, $\mu_0(E_0)$ is the bare atom background, and $\Delta\mu_0(E_0)$ is the step in $\mu(E)$ value at the absorption edge. The energy-dependent absorption coefficient $\chi(E)$ is converted to the wavenumber-dependent absorption coefficient $\chi(k)$ using the relation

$$K = \sqrt{\frac{2m(E - E_0)}{\hbar^2}}$$

where m is the electron mass, $\chi(k)$ is weighted by k^2 to amplify the oscillation at high k, and the $\chi(k)k^2$ functions are Fourier transformed in R space to generate the $\chi(R)$ versus R spectra in terms of the real distances from the center of the absorbing atom (Th). The set of EXAFS data analysis program available within the Demeter software package was used for EXAFS data analysis.[69] The coordination number (N), bond length (R/Å), and disorder factor (σ^2) are used as the fitting parameters with the theoretical spectra using ARTEMIS software to analyze the EXAFS data.

A broad peak centered at 1.9 Å observed in the $\chi(R)$ versus R plots (Figure 4) of all samples corresponds to a bond

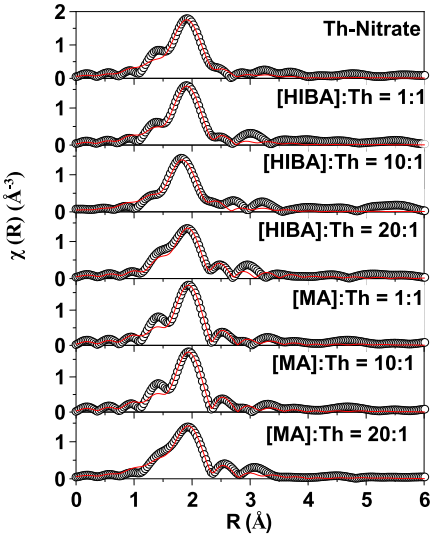

Figure 4. Fourier transform EXAFS spectra at the Th L3 edge for Th-nitrate and Th-HIBA/MA species. Scatter points represent the experimental spectra, and the theoretical fit is represented by red-colored solid lines.

distance of 2.4−2.5 Å, typical for the thorium aqua ion.[70] The coordination number (N), bond length (R/Å), and disorder factor (σ^2) are used as the fitting parameters with the theoretical spectra using ARTEMIS software to analyze the EXAFS data (Table 3). The first peak at 1.9 Å observed for the Th-nitrate system is fitted with two different coordination shells having coordination numbers of 4.43 and 7.37 with Th−O bond distances of 2.43 and 2.55 Å, respectively. Thorium has the ability to form a wide range of complexes ranging from 6 to 12 coordination numbers.[71] EXAFS analysis of the thorium aqua ion showed a coordination of 11.6−12.7 with Th−O bond distances of 2.44−2.46 Å.[70] Neutron and X-ray diffraction studies on the solid thorium nitrate structure reported shorter Th−O bond distances when oxygen from

https://doi.org/10.1021/acsomega.4c01581
ACS Omega 2024, 9, 27289−27299

Table 3. Bond Length, Coordination Number, and Disorder Factor Obtained by EXAFS Fitting at Th L3 Edge

	parameters		Th-HIBA system			Th-MA system		
path	M/L ratio	Th-nitrate	1:1	1:10	1:20	1:1	1:10	1:20
Th−O(I)	R (Å)	2.43 ± 0.01	2.45 ± 0.01	2.41 ± 0.01	2.44 ± 0.01	2.49 ± 0.1	2.42 ± 0.01	2.42 ± 0.01
	N	4.43 ± 0.24	5.29 ± 0.36	5.5 ± 0.29	4.6 ± 0.33	7.82 ± 0.37	4.30 ± 0.28	4.94 ± 0.22
	σ^2	0.002 ± 0.001	0.002 ± 0.001	0.002 ± 0.001	0.002 ± 0.001	0.002 ± 0.001	0.005 ± 0.002	0.003 ± 0.002
Th−O(II)	R (Å)	2.55 ± 0.03	2.56 ± 0.01	2.57 ± 0.02	2.61 ± 0.01	2.72 ± 0.02	2.55 ± 0.02	2.56 ± 0.02
	N	7.4 ± 0.3	4.0 ± 0.3	4.8 ± 0.3	6.0 ± 0.3	4.1 ± 0.3	7.4 ± 0.3	4.9 ± 0.2
	σ^2	0.007 ± 0.002	0.006 ± 0.003	0.007 ± 0.002	0.010 ± 0.003	0.012 ± 0.002	0.011 ± 0.003	0.003 ± 0.002

Table 4. Computed Binding Affinities (kcal/mol)

reaction	HIBA	MA	HIBA	MA
$Th^{4+} + 3L^- \rightarrow [ThL_3]^+$	$[Th(C_4H_7O_3)_3]^+$	$[Th(C_8H_7O_3)_3]^+$	−10.80	+15.65
$Th^{4+} + 4L^- \rightarrow [ThL_4]^+$	$[Th(C_4H_7O_3)_3(C_4H_8O_3)]^+$	$[Th(C_8H_7O_3)_3(C_8H_8O_3)]^+$	−28.40	−76.99
$Th^{4+} + 3L^- + NO_3 \rightarrow [ThL_3NO_3]^-$	$[Th(C_4H_6O_3)_2(C_4H_8O_3)(NO_3)]^-$	$[Th(NO_3)(C_8H_6O_3)(C_8H_7O_3)_2]^-$	−17.83	+8.24
$Th^{4+} + 4L^- \rightarrow [ThL_4]^-$	$[Th(C_4H_7O_3)_3(C_4H_6O_3)]^-$	$[Th(C_8H_7O_3)_3(C_8H_6O_3)]^-$	−40.43	−107.10

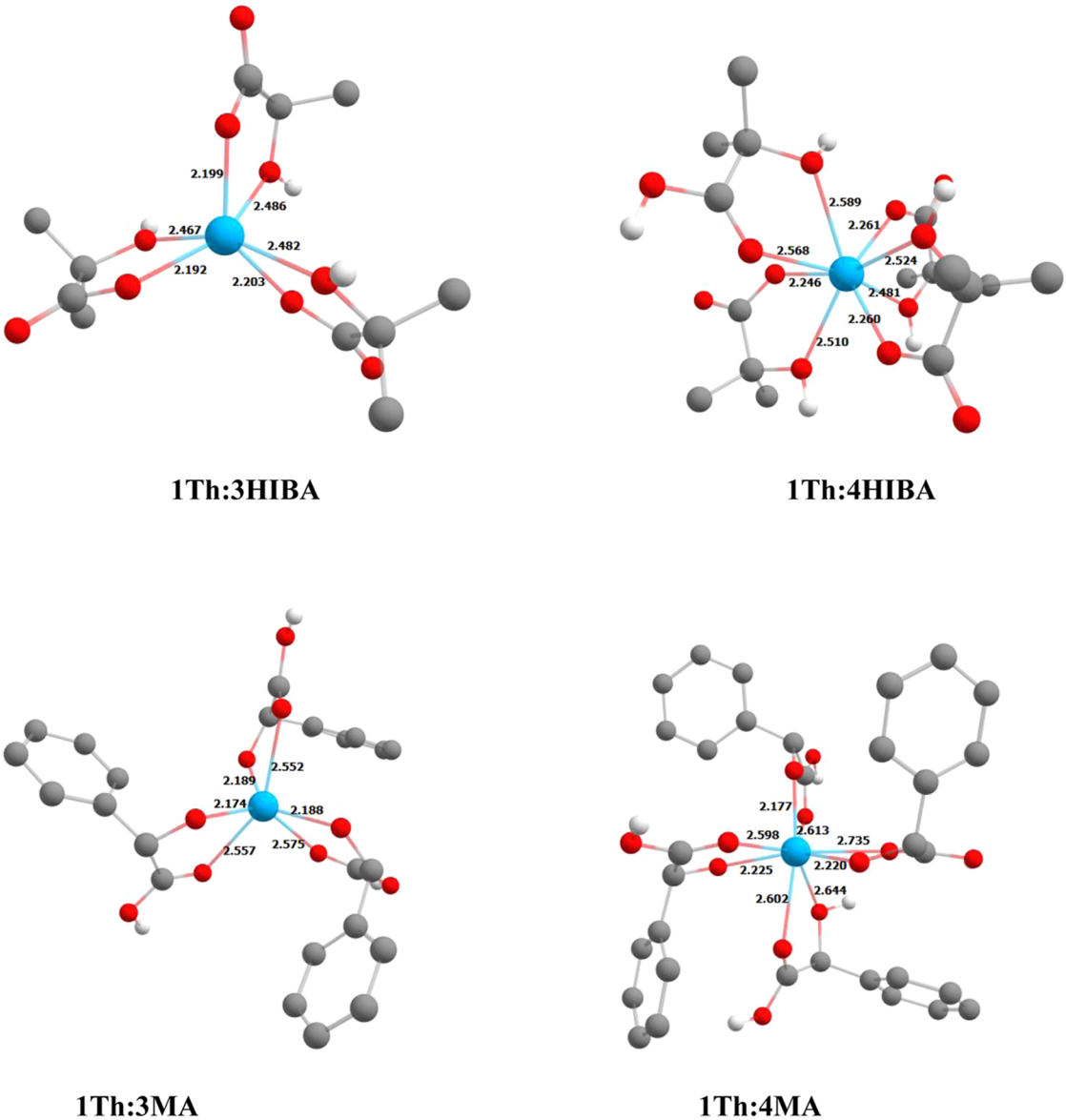

Figure 5. Optimized structures of positively charged species of Th ions with HIBA MA in 1:3 and 1:4 ratios. Blue, uranium; red, oxygen; gray, carbon; bond lengths are in Å.

https://doi.org/10.1021/acsomega.4c01581
ACS Omega 2024, 9, 27289−27299

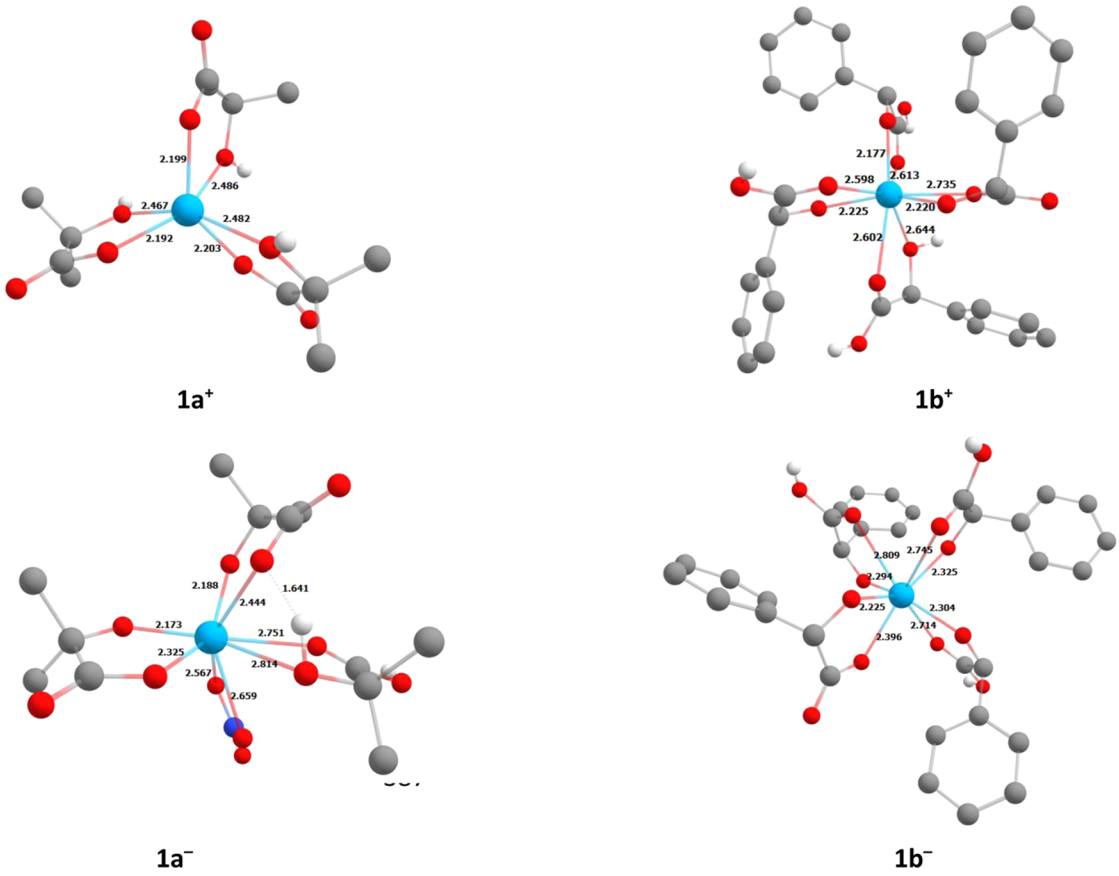

Figure 6. Optimized structures of most stable species in 1Th:3HIBA ($\mathbf{1a}^+$, $\mathbf{1a}^-$) and 1Th:4MA ($\mathbf{1b}^+$, $\mathbf{1b}^-$) in the positive and negative modes. (color code: blue, uranium; red, oxygen; gray, carbon; bond lengths are in Å).

water is bonded (2.43−2.47 Å) than from nitrate (2.53−2.62 Å). Further, the studies showed the bidentate nature of nitrate ions in the structure.[72,73] In the solution phase also, thorium is expected to form bidentate complexes with nitrate ions.[74] The coordination number and Th−O bond distance determined in the present study (Table 3) indicate the mixture of various Th-NO_3−H_2O coordinated species and are in line with experimentally determined thorium tetra nitrate species.[74,75] With the addition of the ligand HIBA/MA, there is a decrease in the coordination number with two different coordination modes, as reflected in the Th−O bond distances (Table 3).

The observation of different binding modes of thorium with carboxylic acid groups, as reported by Zhang et al. in their study on Th-MOFs, highlights the versatility and complexity of metal−ligand interactions.[76] In this finding, interestingly, the presence of various carboxylic groups offers different binding modes to thorium. The others pointed out the bond length of Th and oxygen, which was similar to the findings of the current study. The similarity in the Th−oxygen bond lengths observed in the manuscript to those reported by Tuston et al. for Th coordination complexes, including the Th-(*N*-(2-hydroxyethyl)iminodiacetic acid) (Th-HEIDI) ligand, further supports the notion that Th−oxygen distances can vary within a certain range depending on the specific ligand and coordination environment.[71] This consistency across different studies reinforces our understanding of metal−ligand interactions and provides valuable insights into the structural properties of Th complexes. Chen et al. synthesized lanthanide-HIBA crystals from nitrate salts and showed that lanthanides form a chelate complex by forming two different Ln−O bonds by carboxylate and hydroxyl oxygen atoms, and the complexes behave identically in both solid and solution states.[77] Glycolic acid, a similar hydroxyl carboxylate, is also known to form chelate complexes, and EXAFS analysis of the Th-glycolate complex showed two distinct Th−O bonds corresponding to carboxylate and hydroxyl attachments to central thorium ion.[78] Zhang et al. synthesized the thorium-tetralactato complex and showed that the Th−O bond distances for carboxylate and hydroxyl oxygen are 2.43 and 2.48 Å. respectively, while the Th−O bond distance that arose from water oxygen elongated to 2.54 Å.[79] Thus, the Th−O bond distances at ∼2.45 and ∼2.58 Å obtained in the present studies (Table 3) are attributed to Th−O bond by chelate formation involving both carboxylate and hydroxyl oxygen from HIBA/MA and water, respectively. Although EXAFS cannot differentiate between the oxygen of the hydroxyl group and the carboxylic group, the difference in the bond length indicates that there are two different types of oxygens involved. The consistency of the chelation group across different ligand concentrations suggests that it plays a stable role in complex formation; however, bond lengths were found to vary with a change in the ligand concentration (Figure S2), which may reflect changes in molecular environments or coordination geometries. The optimized bond lengths are plotted against the ligand/metal ratio (Figure S2) for the first two oxygen coordination, contributing to the initial coordination peaks in Figure 4. It is noticeable that relatively shorter bond lengths are observed for a metal/ligand ratio of 1:10. A subsequent increase in bond lengths is observed at an L/M ratio of 20 for the HIBA ligand; however, MA shows a nearly consistent bond

https://doi.org/10.1021/acsomega.4c01581
ACS Omega 2024, 9, 27289−27299

length. This has been further corroborated by DFT calculations.

3.5. Computational Results. The molecular size of HIBA is smaller than that of MA, and it seems logical that 1:4 and 1:3 complexation should be favorable for HIBA and MA extractants, respectively. However, favorable formation of 1:3 and 1:4 species with HIBA and MA in positive and negative modes is found in our ESI-MS and potentiometric experiments. The origin of this differential binding pattern is further scrutinized based on density functional theory (DFT)-based calculations. The initial geometries are built from the stoichiometry derived from ESI-MS data, as shown in Table 4.

Figure 5 shows the most stable 1:3 species of HIBA and 1:4 species of MA in the positive mode. The optimized structures of higher energy species in positive and negative modes are shown in Figure S3. Th(IV) ions react with 3 molecules of HIBA or MA to form the positive ion species through the deprotonation of carboxylate or alcoholic proton, leading to the formation of 1:3 complexes. The most stable species with three HIBA molecules is denoted as $\mathbf{1a}^+$ in Figure 6. For HIBA, deprotonation of the carboxylate group is the most stable species with a favorable binding energy of 10.8 kcal mol^{-1}, as shown in Table 4. The bond length of the Th(IV) ion with the deprotonated carboxylate oxygen is shorter than that of the neutral hydroxo oxygen by ∼0.25 Å, in line with our EXAFS data. The EXAFS-computed Th−O bond length in HIBA is approximately 2.4 Å, which is in line with the DFT bond length for $Th(HIBA)_3$ systems. Similarly, for Th-MA systems, the computed value of 2.7 Å is again in line with the EXAFS data. For 1:3 MA species, we find that deprotonating the hydroxo species binding with Th(IV) ions is the most stable species. Unlike the HIBA complexes, the $Th-O_{OH}$ bond length is shorter than the $Th-O_{COOH}$ species, which is not surprising. These variations lead to favorable formation energies with 1:3 complexes with HIBA in the positive ion mode. Between the two 1:4 extractants with HIBA and MA, we note that the binding free energy of MA ($\mathbf{1b}^+$) is much stronger than HIBA, as shown in Table 4.

The large differences in the computed binding affinity of $\mathbf{1b}^+$ are probably due to their stronger dispersion effect as compared to HIBA. The four phenyl rings of MA interact strongly with each other (<4.0 Å) (Figure S4), and the hydroxyl protons further interact with the phenyl rings (Figure S5). These additional interactions lead to stronger $\pi-\pi$ interactions that are minimal in the corresponding 1:3 complex and absent in the case of the 1:3 and 1:4 HIBA complexes. A similar trend is also noticed in the negative mode.

4. CONCLUSIONS

Hydroxycarboxylates are key constituents of natural organic matter with wide biological activity and industrial applications in the field of separation science. This study shows the detailed speciation of thorium by two hydroxycarboxylates differing by the side chain but similar with respect to the interacting functional groups (−OH, −COOH). The determined stability of species could depict the trends in the variation of elution patterns. Further, a comprehensive ESI-MS identification of a huge number of Th-HIBA/MA species would fill the literature gap in determining all possible products that could result in the interaction of thorium with HIBA or MA. Preliminary data provided by EXAFS and computation shed light on possible coordination modes of these species. The reported study could assist as an addendum or base point for further clarification, and research needs to be carried out on the interaction of lanthanides/actinides, in particular, the tetravalent actinides with molecules containing both carboxylate and hydroxide functional groups. Also, further studies on the interaction of thorium with biologically and naturally available organic moieties were carried out to understand the role of complexation in the transportation and migration of thorium.

■ ASSOCIATED CONTENT

Supporting Information

The Supporting Information is available free of charge at https://pubs.acs.org/doi/10.1021/acsomega.4c01581.

ESI-MS identified species for thorium and HIBA/MA; schematic representations of the formation of different Th-HIBA/MA species identified in both positive and negative ion modes of ESI-MS, and computed structural diagram (PDF)

■ AUTHOR INFORMATION

Corresponding Authors

Mahesh Sundararajan − *Theoretical Chemistry Section, Chemistry Division, Bhabha Atomic Research Centre, Mumbai 400085, India; Homi Bhabha National Institute, Mumbai 400094, India;* orcid.org/0000-0002-1522-124X; Email: smahesh@barc.gov.in

Jaison P. George − *Fuel Chemistry Division, Bhabha Atomic Research Centre, Mumbai 400085, India*; Email: jaipg@barc.gov.in

Authors

Pranaw Kumar − *Fuel Chemistry Division, Bhabha Atomic Research Centre, Mumbai 400085, India*

Rama Mohana Rao Dumpala − *Radiochemistry Division, Bhabha Atomic Research Centre, Mumbai 400085, India; Institute for Nuclear Waste Disposal, Karlsruhe Institute of Technology, 76021 Karlsruhe, Germany;* orcid.org/0000-0003-3891-7001

Vijay M. Telmore − *Fuel Chemistry Division, Bhabha Atomic Research Centre, Mumbai 400085, India*

Biswajit Sadhu − *Health Physics Division, Bhabha Atomic Research Centre, Mumbai 400085, India;* orcid.org/0000-0002-7291-7091

Ashok K. Yadav − *Atomic & Molecular Physics Division, Bhabha Atomic Research Centre, Mumbai 400085, India;* orcid.org/0000-0003-2716-0971

D. Bhattacharyya − *Atomic & Molecular Physics Division, Bhabha Atomic Research Centre, Mumbai 400085, India;* orcid.org/0000-0002-1657-1858

Complete contact information is available at: https://pubs.acs.org/10.1021/acsomega.4c01581

Notes

The authors declare no competing financial interest.

■ ACKNOWLEDGMENTS

P.K. thanks Dr. S. C. Parida, Head, FCD, BARC, for his constant support and encouragement.

■ REFERENCES

(1) *Status and Trends in Spent Fuel and Radioactive Waste Management*; International Atomic Energy Agency: Vienna, 2022.

(2) Xiu, T.; Liu, L.; Liu, S.; Shehzad, H.; Liang, Y.; Zhang, M.; Ye, G.; Jiao, C.; Yuan, L.; Shi, W. Complexation and extraction of trivalent actinides over lanthanides using highly soluble phenanthroline diamide ligands with different side chains. *J. Hazard. Mater.* **2024**, *465*, No. 133508.
(3) Liu, Y.; Wang, C.-Z.; Wu, Q.-Y.; Lan, J.-H.; Chai, Z.-F.; Wu, W.-S.; Shi, W.-Q. Theoretical Insights on the Complexation of Americium(III) and Europium(III) with Diglycolamide- and Dimethylacetamide-Functionalized Calix[4]arenes. *Inorg. Chem.* **2023**, *62* (21), 8179−8187.
(4) Chen, Y.; Zhang, P.; Yang, X.; Guo, Q.; Weng, H.; Chong, H.; Shi, W.; Lin, M. Radiolysis of diamide phenanthroline extractant: exploring the mechanism of HNO3 enhancing the extraction and An/Ln separation performance after irradiation. *Sep. Purif. Technol.* **2023**, *318*, No. 123994.
(5) Wang, S.; Wang, C.; Yang, X.-f.; Yu, J.-p.; Tao, W.-q.; Yang, S.-l.; Ren, P.; Yuan, L.-y.; Chai, Z.-f.; Shi, W.-q. Selective Separation of Am(III)/Eu(III) by the QL-DAPhen Ligand under High Acidity: Extraction, Spectroscopy, and Theoretical Calculations. *Inorg. Chem.* **2021**, *60* (24), 19110−19119.
(6) Ren, P.; Huang, P.-w.; Yang, X.-f.; Zou, Y.; Tao, W.-q.; Yang, S.-l.; Liu, Y.-h.; Wu, Q.-y.; Yuan, L.-y.; Chai, Z.-f.; Shi, W.-q. Hydrophilic Sulfonated 2,9-Diamide-1,10-phenanthroline Endowed with a Highly Effective Ligand for Separation of Americium(III) from Europium(III): Extraction, Spectroscopy, and Density Functional Theory Calculations. *Inorg. Chem.* **2021**, *60* (1), 357−365.
(7) Choppin, G. R.; Silva, R. J. Separation of the lanthanides by ion exchange with alpha-hydroxy isobutyric acid. *J. Inorg. Nucl. Chem.* **1956**, *3*, 153−154.
(8) Smith, H. L.; Hoffman, D. C. Ion-exchange separations of the lanthanides and actinides by elution with ammonium alpha-hydroxy-isobutyrate. *J. Inorg. Nucl. Chem.* **1956**, *3* (3), 243−247.
(9) Nash, K. L.; Jensen, M. P. Analytical-scale Separations of the Lanthanides: A Review of Techniques and Fundamentals. *Sep. Sci. Technol.* **2001**, *36* (5−6), 1257−1282.
(10) Knight, C. H.; Cassidy, R. M.; Recoskie, B. M.; Green, L. W. Dynamic ion exchange chromatography for determination of number of fissions in thorium-uranium dioxide fuels. *Anal. Chem.* **1984**, *56* (3), 474−478.
(11) Cassidy, R. M.; Elchuk, S.; Elliot, N. L.; Green, L. W.; Knight, C. H.; Recoskie, B. M. Dynamic ion exchange chromatography for the determination of number of fissions in uranium dioxide fuels. *Anal. Chem.* **1986**, *58* (6), 1181−1186, DOI: 10.1021/ac00297a045.
(12) Cassidy, R. M.; Chauvel, C. Modern liquid chromatographic techniques for the separation of Nd and Sr for isotopic analyses. *Chem. Geol.* **1989**, *74* (3), 189−200.
(13) Elchuk, S.; Burns, K. I.; Cassidy, R. M.; Lucy, C. A. Reversed-phase separation of transition metals, lanthanides and actinides by elution with mandelic acid. *J. Chromatogr. A* **1991**, *558* (1), 197−207.
(14) Hao, F.; Paull, B.; Haddad, P. R. Retention behaviour of thorium(IV) and uranyl on a reversed-phase column with glycolate and mandelate as eluents. *J. Chromatogr. A* **1996**, *739* (1), 151−161.
(15) Datta, A.; Sivaraman, N.; Viswanathan, K.; Ghosh, S.; Srinivasan, T. G.; Rao, P. Correlation of retention of lanthanide and actinide complexes with stability constants and their speciation. *Radiochim. Acta* **2013**, *101*, 81−92.
(16) Jaison, P. G.; Telmore, V. M.; Kumar, P.; Aggarwal, S. K. Reversed-phase liquid chromatography using mandelic acid as an eluent for the determination of uranium in presence of large amounts of thorium. *J. Chromatogr. A* **2009**, *1216* (9), 1383−1389.
(17) Sundararajan, M.; Rajaraman, G.; Ghosh, S. K. Speciation of uranyl ions in fulvic acid and humic acid: a DFT exploration. *Phys. Chem. Chem. Phys.* **2011**, *13* (40), 18038−18046.
(18) Sadhu, B.; Sundararajan, M.; Bandyopadhyay, T. Water-Mediated Differential Binding of Strontium and Cesium Cations in Fulvic Acid. *J. Phys. Chem. B* **2015**, *119* (34), 10989−10997.
(19) Sundararajan, M.; Ramkumar, J.; Rasu, A.; Venuvanalingam, P. Speciation of Iodide and Iodate Anions in Geochemical Environments: A Theory Driven Experimental Study. *Austin Environ. Sci.* **2023**, *8* (3), No. 1093.
(20) Nardi, S.; Schiavon, M.; Francioso, O. Chemical Structure and Biological Activity of Humic Substances Define Their Role as Plant Growth Promoters. *Molecules* **2021**, *26*, No. 2256, DOI: 10.3390/molecules26082256.
(21) Dusselier, M.; Van Wouwe, P.; Dewaele, A.; Makshina, E.; Sels, B. F. Lactic acid as a platform chemical in the biobased economy: the role of chemocatalysis. *Energy Environ. Sci.* **2013**, *6* (5), 1415−1442.
(22) McKeage, K. Propiverine: a review of its use in the treatment of adults and children with overactive bladder associated with idiopathic or neurogenic detrusor overactivity, and in men with lower urinary tract symptoms. *Clin. Drug Invest.* **2013**, *33* (1), 71−91.
(23) Dusselier, M.; Sels, B. F. Selective Catalysis for Cellulose Conversion to Lactic Acid and Other α-Hydroxy Acids. In *Selective Catalysis for Renewable Feedstocks and Chemicals*; Nicholas, K. M., Ed.; Springer International Publishing: Cham, 2014; pp 85−125.
(24) Yin, Q.; Yin, L.; Wang, H.; Cheng, J. Synthesis and Biomedical Applications of Functional Poly(α-hydroxy acids) via Ring-Opening Polymerization of O-Carboxyanhydrides. *Acc. Chem. Res.* **2015**, *48* (7), 1777−1787.
(25) Sudarsanam, P.; Zhong, R.; Van den Bosch, S.; Coman, S. M.; Parvulescu, V. I.; Sels, B. F. Functionalised heterogeneous catalysts for sustainable biomass valorisation. *Chem. Soc. Rev.* **2018**, *47* (22), 8349−8402.
(26) Gao, C.; Zhang, W.; Ma, C.; Liu, P.; Xu, P. Kinetic resolution of 2-hydroxybutanoate racemic mixtures by NAD-independent L-lactate dehydrogenase. *Bioresour. Technol.* **2011**, *102* (7), 4595−4599.
(27) Bocková, J.; Jones, N. C.; Meierhenrich, U. J.; Hoffmann, S. V.; Meinert, C. Chiroptical activity of hydroxycarboxylic acids with implications for the origin of biological homochirality. *Commun. Chem.* **2021**, *4* (1), No. 86.
(28) da Silva Maffei, R.; Yokoyama-Yasunaka, J. K.; Miguel, D. C.; Uliana, S. R.; Espósito, B. P. Synthesis, characterization and evaluation of antileishmanial activity of copper(II) with fluorinated α-hydroxycarboxylate ligands. *BioMetals* **2009**, *22* (6), 1095−1101.
(29) Wang, Q.; Geng, S.; Wang, L.; Wen, Z.; Sun, X.; Huang, H. Bacterial mandelic acid degradation pathway and its application in biotechnology. *J. Appl. Microbiol.* **2022**, *133* (2), 273−286.
(30) Burns, J.; McCoy, C. P.; Irwin, N. J. Synergistic activity of weak organic acids against uropathogens. *J. Hosp. Infect.* **2021**, *111*, 78−88.
(31) Magon, L.; Bismondo, A.; Maresca, L.; Tomat, G.; Portanova, R. The stability constants of thorium(IV) complexes with α-, β- and γ-hydroxymonocarboxylate ligands in aqueous solution. *J. Inorg. Nucl. Chem.* **1973**, *35* (12), 4237−4243.
(32) Portanova, R.; Lajunen, L. H. J.; Tolazzi, M.; Piispanen, J. Critical evaluation of stability constants for alpha-hydroxycarboxylic acid complexes with protons and metal ions and the accompanying enthalpy changes. Part II. Aliphatic 2-hydroxycarboxylic acids (IUPAC Technical Report). *Pure Appl. Chem.* **2003**, *75* (4), 495−540, DOI: 10.1351/pac200375040495.
(33) Choppin, G. R.; Silva, R. J. Separation of the lanthanides by ion exchange with alpha-hydroxy isobutyric acid. *J. Inorg. Nucl. Chem.* **1956**, *3*, 153−154.
(34) Poswal, A. K.; Agrawal, A.; Yadav, A. K.; Nayak, C.; Basu, S.; Kane, S. R.; Garg, C. K.; Bhattachryya, D.; Jha, S. N.; Sahoo, N. K. In *Commissioning and First Results of Scanning Type EXAFS Beamline (BL-09) at INDUS-2 Synchrotron Source*, AIP Conference Proceedings; AIP, 2014; pp 649−651.
(35) Basu, S.; Nayak, C.; Yadav, A. K.; Agrawal, A.; Poswal, A. K.; Bhattacharyya, D.; Jha, S. N.; Sahoo, N. K. A comprehensive facility for EXAFS measurements at the INDUS-2 synchrotron source at RRCAT, Indore, India. *J. Phys.: Conf. Ser.* **2014**, *493* (1), No. 012032.
(36) Becke, A. D. Density-functional exchange-energy approximation with correct asymptotic behavior. *Phys. Rev. A* **1988**, *38* (6), No. 3098.
(37) Becke, A. D. Density-functional thermochemistry. III. The role of exact exchange. *J. Chem. Phys.* **1993**, *98*, 5648−5652.

https://doi.org/10.1021/acsomega.4c01581
ACS Omega 2024, 9, 27289−27299

(38) Weigend, F.; Ahlrichs, R. Balanced basis sets of split valence, triple zeta valence and quadruple zeta valence quality for H to Rn: Design and assessment of accuracy. *Phys. Chem. Chem. Phys.* **2005**, *7* (18), 3297−3305.
(39) Grimme, S.; Antony, J.; Ehrlich, S.; Krieg, H. A consistent and accurate ab initio parametrization of density functional dispersion correction (DFT-D) for the 94 elements H-Pu. *J. Chem. Phys.* **2010**, *132* (15), No. 154104.
(40) Grimme, S.; Ehrlich, S.; Goerigk, L. Effect of the damping function in dispersion corrected density functional theory. *J. Comput. Chem.* **2011**, *32* (7), 1456−1465.
(41) Misra, N.; Rawat, S.; Tiwari, M.; Bharti, N. K.; Sundararajan, M.; Shelkar, S. A.; Goel, N. K.; Pathak, A.; Kumar, V. Radiation grafting mediated tailoring of a mercury (Hg(II)) selective adsorbent "RAdMer": Mechanistic insights, uptake performance and reusability evaluation in artificially contaminated groundwater. *Groundwater Sustainable Dev.* **2024**, *25*, No. 101139.
(42) Mishra, L.; Sundararajan, M.; Bandyopadhyay, T. MD simulation reveals differential binding of Cm(III) and Th(IV) with serum transferrin at acidic pH. *Proteins: Struct., Funct., Bioinf.* **2021**, *89* (2), 193−206.
(43) Vats, B. G.; Das, D.; Sadhu, B.; Kannan, S.; Pius, I. C.; Noronha, D. M.; Sundararajan, M.; Kumar, M. Selective recognition of uranyl ions from bulk of thorium(iv) and lanthanide(iii) ions by tetraalkyl urea: a combined experimental and quantum chemical study. *Dalton Trans.* **2016**, *45* (25), 10319−10325.
(44) Sundararajan, M.; Sinha, V.; Bandyopadhyay, T.; Ghosh, S. K. Can functionalized cucurbituril bind actinyl cations efficiently? A density functional theory based investigation. *J. Phys. Chem. A* **2012**, *116* (17), 4388−4395.
(45) Sundararajan, M. Redox Potentials of Uranyl Ions in Macrocyclic Complexes: Quantifying the Role of Counter-Ions. *ACS Omega* **2023**, *8* (20), 18041−18046.
(46) Khungar, B.; Roy, A.; Kumar, A.; Sadhu, B.; Sundararajan, M. Predicting the redox properties of uranyl complexes using electronic structure calculations. *Int. J. Quantum Chem.* **2017**, *117* (12), No. e25370.
(47) TURBOMOLE V 7.2, A development of University of Karlsruhe and Forschungszentrum Karlsruhe GmbH, 1989−2015, TURBOMOLE GmBH, 2007. https://www.turbomole.org/.
(48) Ahlrichs, R.; Bär, M.; Häser, M.; Horn, H.; Kölmel, C. Electronic structure calculations on workstation computers: The program system turbomole. *Chem. Phys. Lett.* **1989**, *162* (3), 165−169.
(49) Dumpala, R. M. R.; Boda, A.; Kumar, P.; Rawat, N.; Ali, S. M. Reduction in Coordination Number of Eu(III) on Complexation with Pyrazine Mono- and Di-Carboxylates in Aqueous Medium. *Inorg. Chem.* **2019**, *58* (16), 11180−11194.
(50) Srivastava, A.; Dumpala, R. M. R.; Kumar, P.; Kumar, R.; Rawat, N. Chemical and Redox Speciation of Uranyl with Three Environmentally Relevant Bifunctional Chelates: Multi-Technique Approach Combined with Theoretical Estimations. *Inorg. Chem.* **2022**, *61* (39), 15452−15462.
(51) Dumpala, R. M. R.; Das, S. K.; Ali, M.; Boda, A.; Kumar, P.; Rawat, N.; Kumar, A.; Ali, S. M. Characterization of Thorium-Pyrazinoic acid complexation and its decorporation efficacy in human cells and blood. *Chemosphere* **2021**, *271*, No. 129547.
(52) Dumpala, R. M. R.; Rao, M.; Rawat, N.; Sawant, R.; Manna, D.; Ghanty, T.; Tomar, B. Thermodynamic study of Eu(III) complexation by pyridine monocarboxylates. *J. Chem. Thermodyn.* **2012**, *55*, 67−74, DOI: 10.1016/j.jct.2012.06.017.
(53) Rao, D. R. M.; Rawat, N.; Manna, D.; Sawant, R. M.; Ghanty, T. K.; Tomar, B. S. Complexation of thorium with pyridine monocarboxylates: A thermodynamic study by experiment and theory. *J. Chem. Thermodyn.* **2013**, *58*, 432−439.
(54) Dumpala, R. M. R.; Rawat, N.; Bhattacharya, A.; Tomar, B. S. Coordination Modes of Hydroxamates in Neptunium (V) Complexes in Aqueous Solution. *ChemistrySelect* **2017**, *2* (9), 2722−2731.
(55) Sharma, S.; Dumpala, R. M. R.; Rawat, N. Solution Thermodynamics for the Thorium Complexation with N-(2-Hydroxyethyl) Iminodiacetic Acid. *J. Chem. Eng. Data* **2020**, *65* (6), 2927−2937.
(56) Dumpala, R. M. R.; Rawat, N.; Tomar, B. S. Protonation of Pyridine Monocarboxylate-N-Oxides − Determination of Thermodynamic, Absorbance and Ion Interaction Parameters. *ChemistrySelect* **2017**, *2* (2), 820−829.
(57) Srivastava, A.; Dumpala, R. M. R.; Rawat, N.; Tomar, B. S. Electrochemical, spectroscopic and theoretical studies on redox speciation of neptunium with phenylphosphonic acid. *Inorg. Chim. Acta* **2018**, *482*, 307−316.
(58) Dumpala, R. M. R.; Rawat, N.; Tomar, B. S. Stability, speciation and spectral properties of NpO2+ complexes with pyridine monocarboxylates in aqueous solution. *Spectrochim. Acta, Part A* **2017**, *181*, 13−22.
(59) Dumpala, R. M. R.; Srivastava, A.; Rawat, N. Experimental and theoretical approach to probe the aquatic speciation of transuranic (neptunyl) ion in presence of two omnipresent organic moieties. *Chemosphere* **2021**, *273*, No. 129745.
(60) Sharma, S.; Dumpala, R. M. R.; Yadav, A. K.; Rawat, N. Aquatic speciation of Eu(III) with N-(hydroxyl ethyl)iminodiacetic acid (HEIDA), a major degradation product of organic radioactive waste. *J. Environ. Chem. Eng.* **2021**, *9* (6), No. 106584.
(61) Dumpala, R. M. R.; Sharma, S.; Boda, A.; Rawat, N.; Ali, S. M. The aqueous interaction of neodymium with two omni existent biomoieties − a mechanistic understanding by experimental and theoretical studies. *Dalton Trans.* **2021**, *50* (44), 16191−16204.
(62) Dumpala, R. M. R.; Rawat, N.; Boda, A.; Ali, S. M.; Tomar, B. S. Complexation of thorium with pyridine monocarboxylate-N-oxides: Thermodynamic and computational studies. *J. Chem. Thermodyn.* **2018**, *122*, 13−22.
(63) Dumpala, R. M. R.; Rawat, N.; Boda, A.; Ali, S. M.; Tomar, B. S. Structural, luminescence, thermodynamic and theoretical studies on mononuclear complexes of Eu(III) with pyridine monocarboxylate-N-oxides in aqueous solution. *Spectrochim. Acta, Part A* **2018**, *190*, 150−163.
(64) Dumpala, R. M. R.; Srivastava, A.; Sharma, S.; Rawat, N. Protonation of Phosphonocarboxylates in Aqueous Medium: An Experimental and Theoretical Investigation. *J. Chem. Eng. Data* **2022**, *67* (9), 2174−2181.
(65) Gans, P.; Sabatini, A.; Vacca, A. Investigation of equilibria in solution. Determination of equilibrium constants with the HYPERQUAD suite of programs. *Talanta* **1996**, *43* (10), 1739−1753.
(66) Raut, N. M.; Jaison, P. G.; Aggarwal, S. K. Comparative evaluation of three α-hydroxycarboxylic acids for the separation of lanthanides by dynamically modified reversed-phase high-performance liquid chromatography. *J. Chromatogr. A* **2002**, *959* (1), 163−172.
(67) Kumar, P.; Jaison, P. G.; Telmore, V. M.; Sadhu, B.; Sundararajan, M. Speciation of uranium-mandelic acid complexes using electrospray ionization mass spectrometry and density functional theory. *Rapid Commun. Mass Spectrom.* **2017**, *31* (6), 561−571.
(68) *X-Ray Absorption: Principles, Applications, Techniques of EXAFS, SEXAFS and XANES.*; Koningsberger, D. C.; Prins, R., Eds.; Wiley, 1988.
(69) Newville, M.; Ravel, B.; Haskel, D.; Rehr, J. J.; Stern, E. A.; Yacoby, Y. Analysis of multiple-scattering XAFS data using theoretical standards. *Phys. B* **1995**, *208−209*, 154−156.
(70) Rothe, J.; Denecke, M. A.; Neck, V.; Müller, R.; Kim, J. I. XAFS investigation of the structure of aqueous thorium(IV) species, colloids, and solid thorium(IV) oxide/hydroxide. *Inorg. Chem.* **2002**, *41* (2), 249−258.
(71) Tutson, C. D.; Gorden, A. E. V. Thorium coordination: A comprehensive review based on coordination number. *Coord. Chem. Rev.* **2017**, *333*, 27−43.
(72) Ueki, T.; Zalkin, A.; Templeton, D. H. Crystal structure of thorium nitrate pentahydrate by X-ray diffraction. *Acta Crystallogr.* **1966**, *20* (6), 836−841.

https://doi.org/10.1021/acsomega.4c01581
ACS Omega 2024, 9, 27289−27299

(73) Taylor, J. C.; Mueller, M. H.; Hitterman, R. L. Crystal structure of thorium nitrate pentahydrate by neutron diffraction. *Acta Crystallogr.* **1966**, *20* (6), 842−851.
(74) Di Bernardo, P.; Zanonato, P.; Rao, L.; Bismondo, A.; Endrizzi, F. Interaction of thorium(iv) with nitrate in aqueous solution: medium effect or weak complexation? *Dalton Trans.* **2011**, *40* (36), 9101−9105.
(75) Skanthakumar, S.; Jin, G. B.; Lin, J.; Vallet, V.; Soderholm, L. Linking Solution Structures and Energetics: Thorium Nitrate Complexes. *J. Phys. Chem. B* **2017**, *121* (36), 8577−8584.
(76) Zhang, N.; Sun, L.-X.; Bai, F.-Y.; Xing, Y.-H. Thorium−Organic Framework Constructed with a Semirigid Triazine Hexacarboxylic Acid Ligand: Unique Structure with Thorium Oxide Wheel Clusters and Iodine Adsorption Behavior. *Inorg. Chem.* **2020**, *59* (6), 3964−3973.
(77) Chen, X.-Y.; Goff, G. S.; Ewing, W. C.; Scott, B. L.; Runde, W. Solid-State and Solution-State Coordination Chemistry of Lanthanide(III) Complexes with α-Hydroxyisobutyric Acid. *Inorg. Chem.* **2012**, *51* (24), 13254−13263.
(78) Toraishi, T.; Farkas, I.; Szabó, Z.; Grenthe, I. Complexation of Th(iv) and various lanthanides(iii) by glycolic acid; potentiometric, 13C-NMR and EXAFS studies. *J. Chem. Soc., Dalton Trans.* **2002**, No. 20, 3805−3812.
(79) Zhang, Y.; Karatchevtseva, I.; Kadi, F.; Lu, K.; Yoon, B.; Price, J.; Li, F.; Lumpkin, G. Synthesis, spectroscopic characterization and crystal structures of thorium(IV) mononuclear lactato and hexanuclear formato complexes. *Polyhedron* **2015**, *87*, 377−382, DOI: 10.1016/j.poly.2014.12.006.

https://doi.org/10.1021/acsomega.4c01581
ACS Omega 2024, 9, 27289−27299